

INVITED PRESENTATION

# GaAs/AlGaAs Based Multi-Quantum Well Infrared Detector Arrays for Low-Background Applications

Sarath Gunapala, Sumith Bandara, James Bock, Michael Ressler, John Liu, Jason Mumolo, Sir Rafol, Michael Werner, and David Cardimona\*

Jet Propulsion Laboratory, California Institute of Technology  
4800, Oak Grove Drive, Pasadena, CA 91109

\*Air Force Research Laboratory, Kirtland Air Force Base, NM 87117

## ABSTRACT

A long-wavelength large format Quantum Well Infrared Photodetector (QWIP) focal plane array has been successfully used in a ground based astronomy experiment. QWIP arrays afford greater flexibility than the usual extrinsically doped semiconductor infrared (IR) arrays. Recently, we operated an infrared camera with a 256x256 QWIP array sensitive at 8.5  $\mu\text{m}$  at the prime focus of the 5-m Hale telescope, obtaining the images. The remarkable noise stability – and low 1/f noise – of QWIP focal plane arrays enable camera to operate by modulating the optical signal with a mod period up to 100 s. A 500 s observation on dark sky renders a flat image with little indication of the low spatial frequency structures associated with imperfect sky subtraction or detector drifts. At low operating temperatures for low-background irradiance levels, high resistivity of thick barriers in the active region of QWIPs impedes electrons from entering the detector from the opposite electrode. This could lead to a delay in refilling the space-charge buildup, and result in a lower responsivity at high optical modulation frequencies. In order to overcome this problem we have designed a new detector structure, the blocked intersubband detector (BID) with separate active quantum well region and blocking barrier.

## 1. INTRODUCTION

Spectral coverage of conventional interband infrared (IR) detectors are entirely determined by the bandgap because photoexcitation occurs across the band gap ( $E_g$ ) from the valence to conduction band. Therefore, detection of mid wavelength (8-15  $\mu\text{m}$ ) IR radiation requires small bandgap materials such as  $\text{Hg}_{1-x}\text{Cd}_x\text{Te}$  and  $\text{Pb}_{1-x}\text{Sn}_x\text{Te}$ , in which the energy gap can be controlled by varying  $x$ . It is well known that these low band gap materials are more difficult to grow and process than large band gap semiconductors such as GaAs. Thus, it is extremely difficult to produce them in large format uniform arrays. Quantum Well Infrared Photodetectors (QWIPs) avoid such difficulties because they are fabricated using high bandgap materials systems such as  $\text{GaAs}/\text{Al}_x\text{Ga}_{1-x}\text{As}$ <sup>1-4</sup>. It can provide highly uniform, large format focal plane array at lower cost enabling observation covering large areas. Cameras utilizing QWIP FPAs as large as 640 x 486 format arrays have been demonstrated with corrected uniformity better than 99.95%<sup>3,4</sup>. Due to use of artificially created band structure, spectral band width of these detectors can be tailored from narrow ( $\Delta\lambda/\lambda \sim 10\%$ ) to wide ( $\Delta\lambda/\lambda \sim 50\%$ ) in the wavelength range between 4-20  $\mu\text{m}$  allowing various applications<sup>5</sup>. In addition, recent demonstration of the simultaneously readable, dual band, 640x486 QWIP FPA will provide innovative ways of simplify IR sensing instruments<sup>6</sup>.

## 2. QWIP OPERATING PRINCIPLE

QWIPs operate by photoexcitation of electrons between ground and first excited state subbands of multi-quantum wells (MQWs) which are artificially fabricated by placing thin layers of two different, high-bandgap semiconductor materials alternately<sup>1,2</sup>. The bandgap discontinuity of two materials creates quantized subbands in the potential wells associated with conduction bands or valence bands. The structure parameters are designed so that the photo-excited carriers can escape from the potential wells and be collected as photocurrent. See Fig. 1.

The absolute responsivity  $R(\lambda)$  of a QWIP can be written in terms of absorption quantum efficiency ( $\eta_a(\lambda)$ ) and photoconductive gain ( $g$ ) as,  $R(\lambda) = (e/h\nu)\eta_a(\lambda)g^{1,2}$ . Typical absorption quantum efficiency of a QWIPs is  $\eta_a(\lambda) \sim 10\%-30\%$ , and directly proportional to carrier doping density of the multi-quantum well structure. Photoconductive gain of a QWIP detector is determined by the position of the excited state relative to the barrier and the number of quantum wells in the structure<sup>7,8</sup>. For a typical 50 quantum well bound-to-quasibound QWIP, photoconductive gain  $g$  varies from  $\sim 10\%$  to  $\sim 50\%$  with the operating bias voltage. The net quantum efficiency (quantum efficiency and gain product) of a QWIP is reduced due to less than 100% gain resulting a lower photocurrent. However, resulting signal to noise ratio do not reduced by the same factor because both dark current and noise of the detector will be reduced due to the same reason. Also, it is important to note that, background-limited sensitivity is *independent* of photoconductive gain  $g$ .

### 3. SPECTRAL TUNABILITY

Spectral responsivity peak wavelength ( $\lambda_p$ ) of a QWIP is determined by the energy difference between ground and excited states of the quantum well. Unlike the responsivity spectra of intrinsic infrared detectors, QWIPs spectra are much narrower and sharper due to their resonance intersubband absorption. Typically, responsivity spectra of the *bound* and *quasibound* excited state QWIPs are much narrower ( $\Delta\lambda/\lambda \sim 10\%$ ) than the *continuum* QWIPs ( $\Delta\lambda/\lambda = 24\%$ )<sup>1,2</sup>. This is due to the fact that, when the excited state is placed in the continuum band above the barrier, the energy width associated with the state becomes wide. Spectral band width of these QWIPs can be further increased by replacing single quantum wells with small superlattice structures (several quantum wells separated by thin barriers) in the multi-quantum well structure<sup>5</sup>. Such a scheme creates an excited state miniband due to overlap of the excited state wavefunctions of quantum wells. Energy band calculations based on a two band model shows excited state energy levels spreading greater than 30 meV<sup>5</sup>. Figure 3 shows experimentally measured responsivity spectra with 50% bandwidth  $\Delta\lambda > 5 \mu\text{m}^5$ . See Figure 4. Thus, control of the processing allows us to tailor the QWIP characteristics to the specific application in hand.

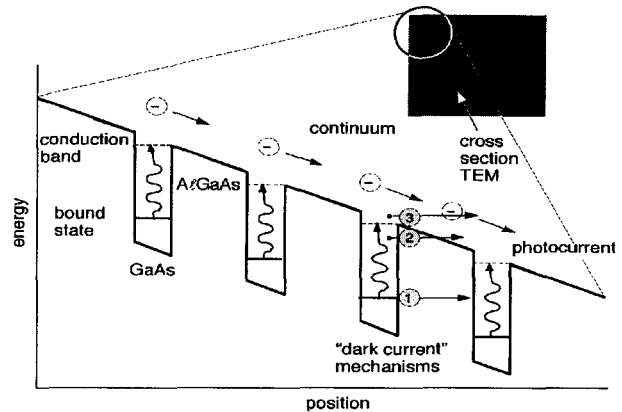


Fig. 1: Schematic diagram of the conduction band in a bound-to-quasibound QWIP in an externally applied electric field. Absorption of IR photons can photoexcite electrons from the ground state of the quantum well into the continuum, causing a photocurrent. Three dark current mechanisms are also shown: ground state tunneling (1); thermally assisted tunneling (2); and thermionic emission (3).

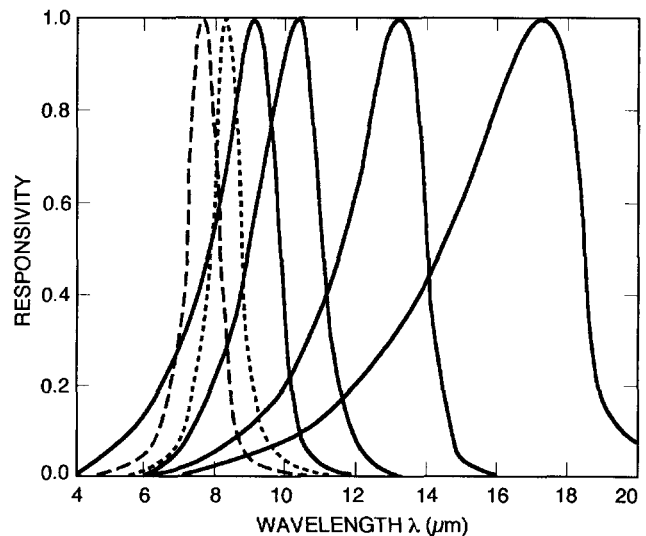


Fig. 2: This figure shows the spectral coverage and tailorability of QWIPs in 4-20  $\mu\text{m}$  wavelength range. The lattice matched GaAs/ $\text{Al}_x\text{Ga}_{1-x}\text{As}$  material system is commonly used to create a QWIP structures similar to the one shown in Figure 1. Highly uniform and pure crystal layers of such semiconductors can be grown on large substrate wafers, with control of each layer thickness down to a fraction of a molecular layer, using modern crystal-growth methods like molecular beam epitaxy (MBE). Thus, by controlling the quantum well width and the barrier height (which depends on the Al molar ratio of  $\text{Al}_x\text{Ga}_{1-x}\text{As}$  alloy), this intersubband transition energy can be varied over a wide enough range to enable light detection at any wavelength range between 4-20  $\mu\text{m}^{1-5}$ .

#### 4. QWIP FPAS FOR ASTRONOMY

One can improve the absorption quantum efficiency by adding more carriers into the quantum wells 1,2. However, carrier density cannot be increased boundlessly because it leads to a higher dark current, which degrades the performance of the detector. The dominant noise in QWIP devices is due to the shot noise resulting from the dark current in the device<sup>2,7,8</sup>. Therefore, it is required to find the optimum  $N_D$  within the given constraints of the application. As shown in the Figure 1, the dark current originates from three main processes; well to well quantum mechanical tunneling, thermally assisted tunneling, and classical thermionic emission. Consequently, for QWIPs operating at higher temperatures, the last mechanism is the major source of dark current. The classical thermionic emission, which can be expressed as  $I_t \propto e^{-\Delta E / kT}$ , where  $\Delta E$  is the effective barrier height measured from the ground state Fermi level, and  $T$  is the operating temperature, decreases exponentially with decreasing operating temperature. If a detector operates at lower temperature, one can improve the photosignal of the detector by adding more carriers to the multi-quantum well structure, regardless of any increase in dark current<sup>9</sup>. Further reduction in low temperature dark current can be achieved by introducing slightly upward graded barriers to multi quantum well structure. This can be achieved easily during the MBE growth of the wafers by slightly increasing the Al concentrations while growing the barriers. These upward graded barriers experience a lower effective electric field than the typical rectangular barriers under an applied bias voltage. This leads to a smaller effective barrier lowering for graded barrier structures, yielding a lower dark current. Fig. 4 shows the predicted dark current as a function of wavelength and temperature for both graded and typical QWIP structures. Note that for the graded QWIP the predicted dark current is less than 10 e/s at all wavelengths shortward of 15 $\mu\text{m}$  for  $T \sim 25\text{K}$ . Such improvements would enable such applications as the Outer Solar System Explorer and enhance the usefulness of QWIPs for spectroscopic applications.

Two high performance QWIP focal plane arrays have been designed for ground-based mid-infrared camera QWICPIC (QWIP Wide-field Imaging multi-Color Prime-focus Infrared Camera) operated at the prime focus of the 5-m Hale telescope at Mt. Palomar<sup>10</sup>.

QWICPIC is specifically designed to take advantage of the large format, narrow band, low 1/f noise, and excellent linearity and noise performance of QWIP arrays under high background conditions. This prime focus camera is designed to image a large 2' x 2' field simultaneously onto three large format focal plane arrays. QWICPIC currently houses dichroic optics enabling observations with 3 focal plane arrays simultaneously at 4.7, 8.5, and 12.5 $\mu\text{m}$ . The optics was

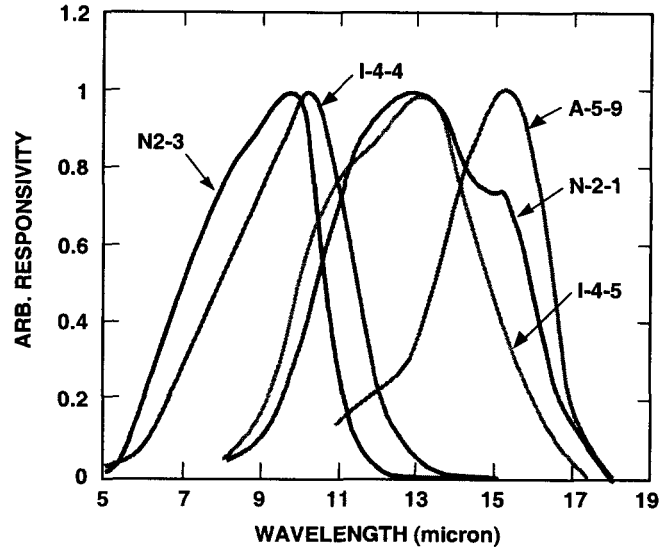


Fig. 3: Spectral responsivity of several broad-band QWIPs which shows spectral coverage and tailorability of QWIPs in 4-20  $\mu\text{m}$  wavelength range.

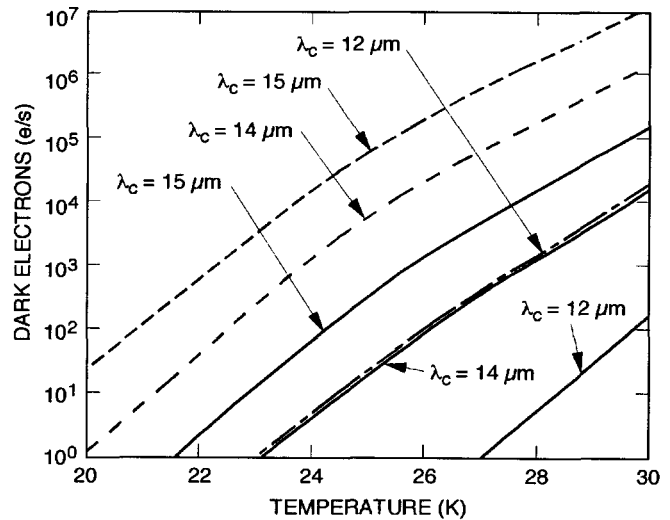


Fig. 4: Estimated low temperature ( $T = 20 - 30\text{K}$ ) dark current per  $40 \times 40\ \mu\text{m}^2$  pixel as a function of cut-off wavelength of graded barrier bound-to-quasi-bound QWIPs. The detectors represent by solid lines are doped to a density of  $N_D = 8 \times 10^{17}\ \text{cm}^{-3}$  and expected achieve 25% peak absorption quantum efficiency. The detectors represent by dashed lines are doped to a density of  $N_D = 1.4 \times 10^{18}\ \text{cm}^{-3}$  and expected achieve higher peak quantum efficiency and broader responsivity.

designed to simultaneously optimized the image quality at the focal plane and the image quality of the pupil stop on the primary mirror. The FPAs are thermally isolated to operate at  $\sim 30$  K.

The QWIP FPA device structures consist of 30 quantum well periods, each period containing a GaAs well and a  $\text{Al}_x\text{Ga}_{1-x}\text{As}$  barrier, sandwiched between top and bottom contact layers doped  $n = 5 \times 10^{17} \text{ cm}^{-3}$ , grown on a semi-insulating GaAs substrate. The cap layer on top of a stop-etch layer was grown *in situ* on top of the device structure to fabricate the light coupling 2-D grating structure<sup>3,4</sup>. The GaAs quantum well thickness and Al concentration ( $x$ ) of  $\text{Al}_x\text{Ga}_{1-x}\text{As}$  barriers of the two devices were optimized to respond in 8-9 and 12-13  $\mu\text{m}$  spectral bands while operating in bound-to-continuum mode. Figure 5 shows the measured responsivity spectrum of each detector. Due to lower operating temperatures, dark currents were suppressed and both devices operate above back ground limited conditions. Figure 5 also shows the peak responsivity vs bias voltage dependence for both devices. These responsivities show about six fold enhancement over previously demonstrated FPAs which were designed for higher operating temperatures<sup>3</sup>. Figure 6 shows the peak detectivity  $D^*$  vs operating temperatures for a background equivalent to QWICPIC operating at the prime focus of the Mt. Palomar 5-m Hale Telescope.

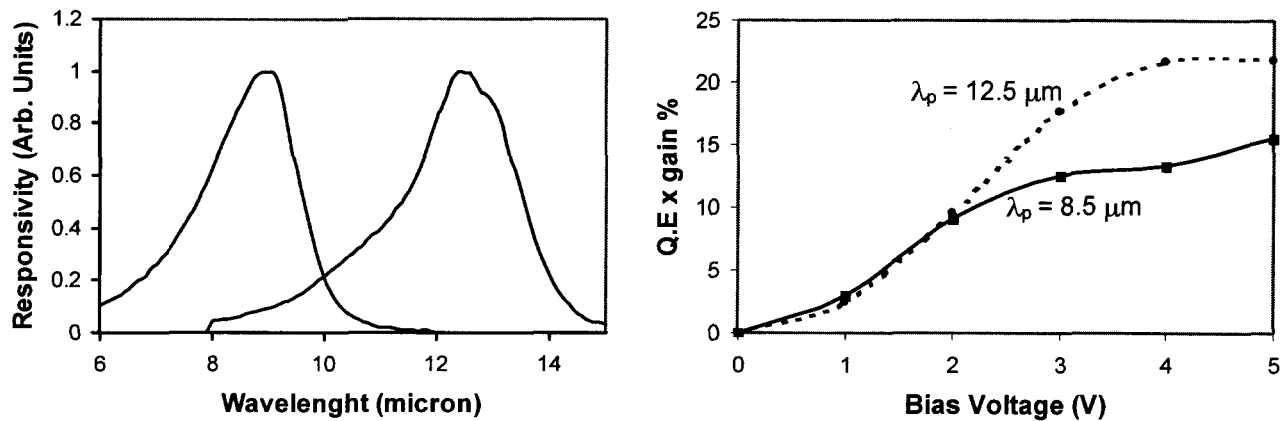


Fig. 5: Measured spectral responsivity and peak quantum efficiency gain product of two QWIP FPAs design for QWICPIC camera operated at the prime focus of the 5-m Hale telescope at Mt. Palomar.

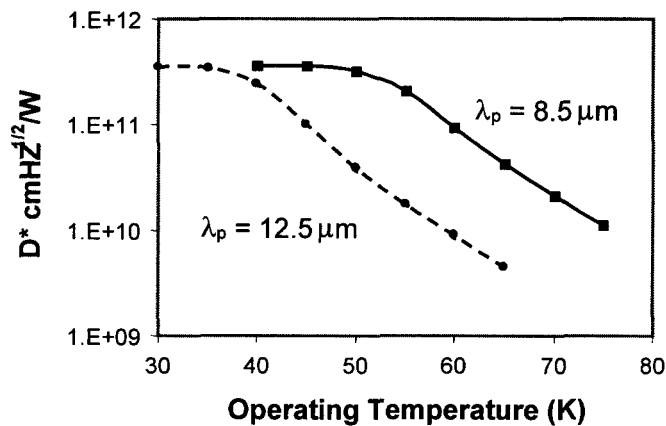


Fig. 6: Peak detectivity  $D^*$  vs operating temperatures for a background equivalent to QWICPIC operating at the prime focus of the Mt. Palomar 5-m Hale Telescope. The photon flux is 20% of 300 K,  $f/3.3$  background.

First science grade 256 x 256 focal plane array was developed using the 8-9  $\mu\text{m}$  QWIP wafer described in the previous paragraph and implemented in the QWICPIC camera. The excellent photometric and noise characteristics of the 256 x 256 QWIP focal plane array allow QWICPIC to observe at the prime focus of the 5-m Hale telescope. As shown in Fig. 7, the lack of  $1/f$  noise above 10 mHz allows for slow modulation and scanning strategies commonly required in space-borne applications. The images shown in Fig. 8 were obtained with minimal data processing: coaddition of frames, sky subtraction, removal of hot pixels, and smoothing in the case of NGC 1068. Faint structures,  $10^4$  times fainter than the brightest source, are apparent with no noticeable bleeding of bright sources or other non-photometric effects. The faint ring around NGC 1068 was imaged in 2400 s at a sensitivity of 3 mJy in a 1" beam. The remarkable noise stability – and low  $1/f$  noise – of QWIP focal plane arrays enable QWICPIC to operate by modulating the optical signal with a nod

period up to 100 s (see Fig.3). A 500 s observation on dark sky renders a flat image with little indication of the low spatial frequency structures associated with imperfect sky subtraction or detector drifts. To our knowledge, QWICPIC represents both the first 256 x 256 mid-infrared imager and the first successful example of a ground-based instrument using slow-nod modulation at mid-infrared wavelengths. We operate QWICPIC at the Palomar telescope without the high frequency background subtraction usually implemented for thermal infrared astronomy via a chopping secondary mirror. Instead, the subtraction was carried out at low frequency by nodding the telescope once per 30 seconds over an angle of  $\sim 5$  arcmin. The resulting high quality image reflects the excellent low frequency noise performance of this device (Fig. 7). This could be a valuable attribute in an Explorer-class mission or NGST for which fiscal constraints might mitigate against either a chopping/scanning mirror or a particularly agile attitude control system. To our knowledge, QWICPIC represents both the first 256 x 256 mid-infrared imager and the first successful example of a ground-based instrument using slow-nod modulation at mid-infrared wavelengths.

### 5. BLOCKED INTER-SUBBAND DETECTOR (BID)

Although QWIP performs exceptionally well under high background levels, the detectors exhibit anomalous behavior when it operates under stringent low irradiance and low temperature conditions (i.e. at extremely low photocurrent). Singh *et al.* have modeled and explained some of the irregular behaviors by treating QWIP as a resistance in series with a capacitance<sup>11,12</sup>. Arrington *et al.*<sup>13</sup> have shown experimentally the non-flat frequency response curves of QWIP at low background and low operating temperature conditions. Under such conditions, responsivity decreases as the detector operating frequency increases. The roll-off frequency is completely determined by the device design and operational conditions<sup>12</sup>. This behavior is empirically similar to dielectric relaxation effects observed in bulk extrinsic silicon and germanium photoconductors under similar operational conditions<sup>14,15</sup>.

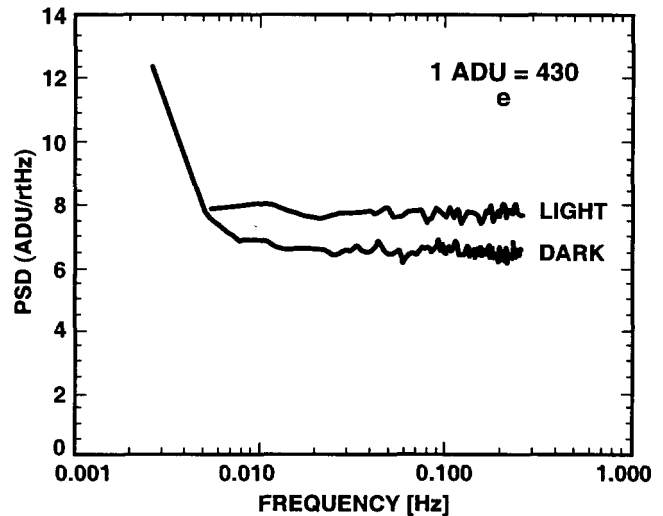


Fig. 7: Noise spectral density of a 8-9  $\mu\text{m}$  256 x 256 QWIP focal plane array (1 ADU = 430  $e^-$ ). The lack of  $1/f$  noise above 10 mHz allows for slow modulation and scanning strategies commonly required in space-borne applications. QWICPIC exploits this advantage in operating at the prime focus by modulating the optical signal with a slow nod period of 20 – 100 s.

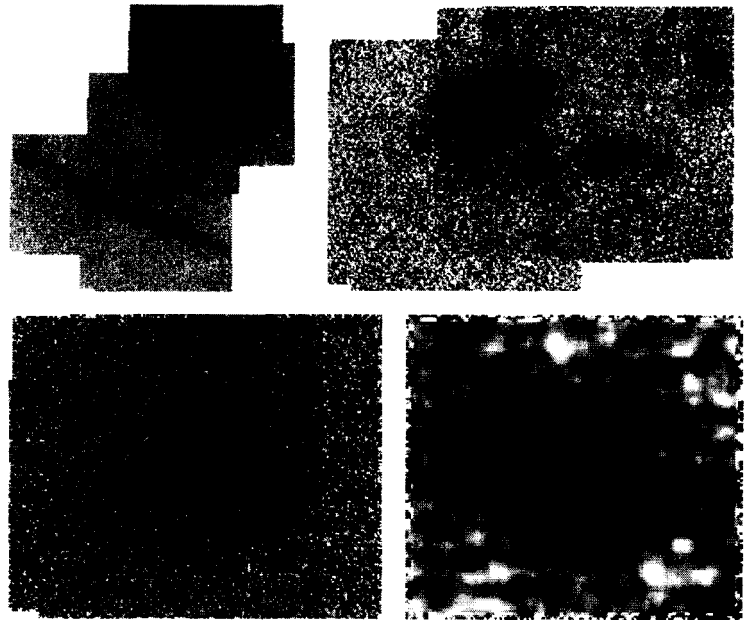


Fig. 8: Mid-infrared images of a) (top left) the Orion nebula, including the bright BN-KL object in the upper right-hand corner, the Trapezium cluster and nebula, and a shock front in the lower left-hand corner b) (top right) the Monoceros R2 star forming region, c) (bottom left) the W3 star forming region, and d) (bottom right) the faint infrared ring of NGC 1068. The images were obtained in a single night with QWICPIC using a 256 x 256  $8.5 \mu\text{m}$  QWIP focal plane array in integration times of 550 – 2400 s on the sky with nod periods of 15 – 20 s. The data are scaled logarithmically in this display to enhance low surface brightness regions.

In principle, QWIP operates very similar to extrinsic bulk photoconductors. Electrons in the subbands of the isolated quantum wells can be visualized as electrons attached to impurity states in bulk photoconductors. As photogenerated electrons depart the active doped quantum well region, they leave behind a space-charge buildup. Thus, in order to operate QWIP steadily, it requires a sufficient dark or background photo current to replenish the depleted quantum wells. This is not an issue for QWIP detectors operating at high background conditions or high temperatures, because high photocurrent or high dark current can easily provide carriers to re-fill the space-charge buildup. However, at low operating temperatures for low-background irradiance levels, high resistivity of thick barriers in the active region impedes electrons from entering the detector from the opposite electrode. This could lead to a delay in refilling the space-charge buildup, and result in a lower responsivity at high optical modulation frequencies. In order to overcome this problem we have designed a new detector structure, the blocked intersubband detector (BID) with separate active quantum well region and blocking barrier. As shown in the Figure 9, the active region of BID consists of quantum wells separated by thin barriers, which creates sub-minibands due to large overlap of sublevel wave functions. Thus, space-charge buildup will get quickly refilled by electrons via sequential resonant tunneling along the ground state miniband from the emitter contact layer. A thick, impurity free blocking barrier is placed between the active region and collector to suppress the dark current of the device.

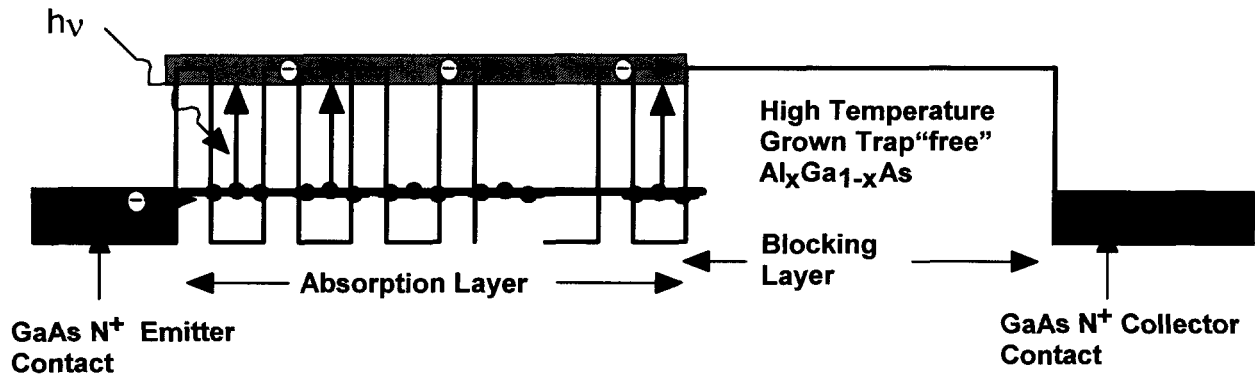


Fig. 9: Energy band diagram of GaAs/AlGaAs blocked intersubband detector. Noise spectral density of a 8-9  $\mu\text{m}$  256 x 256 QWIP focal plane array (1 ADU = 430  $e^-$ ). The lack of 1/f noise above 10 mHz allows for slow modulation and scanning strategies commonly required in space-borne applications. QWICPIC exploits this advantage in operating at the prime focus by modulating the optical signal with a slow nod period of 20 – 100 s.

We have fabricated a BID device consisting of 50 period MQW photosensitive region and a 1  $\mu\text{m}$  thick  $\text{Al}_{1.2}\text{Ga}_{0.2}\text{As}$  blocking barrier layer. Each quantum well period contains a 60  $\text{\AA}$  GaAs well and 100  $\text{\AA}$   $\text{Al}_{1.2}\text{Ga}_{0.2}\text{As}$  barrier. The whole device structure is sandwiched between two GaAs contact layers. (Fig. 9) The sample was grown on a semi-insulating GaAs substrate by molecular beam epitaxy. Transport carriers (electrons) were provided by doping all GaAs wells and contact layers with Si to a density of  $n = 4 \times 10^{17} \text{ cm}^{-3}$ . 200  $\mu\text{m}$  diameter mesas were fabricated using wet chemical etching in order to measure dark current-voltage curves, spectral responsivity and noise. The responsivity spectra of these detectors were measured using a 1000 K blackbody source and a grating monochromator. To obtain normalized responsivity spectra at different bias voltages, detectors were back illuminated through a 45° polished facet<sup>4,5</sup>. Then the absolute spectral responsivities were calculated by measuring total photocurrent due to a calibrated black-body source. Fig. 10 shows responsivity curves at different bias voltages from  $V_B = -0.5$  to 1.5 V. Unlike in typical QWIPs, spectral response of BID shows extra broadening because the photoexcitation occurs between sub-minibands instead of localized sub-levels. Figure 10 also illustrates the absorption quantum efficiency spectrum of the BID, measured using a 45° wave guide geometry<sup>2</sup>.

Although the BID shows comparable absorption quantum efficiency, it shows much smaller responsivity than thick barrier QWIP device. Therefore, photoconductive gain of the BID ( $g = 0.06$  at  $V = -1$  V bias voltage) is a few times smaller ( $g \sim 0.2 - 0.5$  at  $V = -3$  V bias voltage). This can be attributed to the lower electric field across the active region of the BID. Due to higher resistivity of the blocking layer, compared to the active superlattice, much of the applied bias

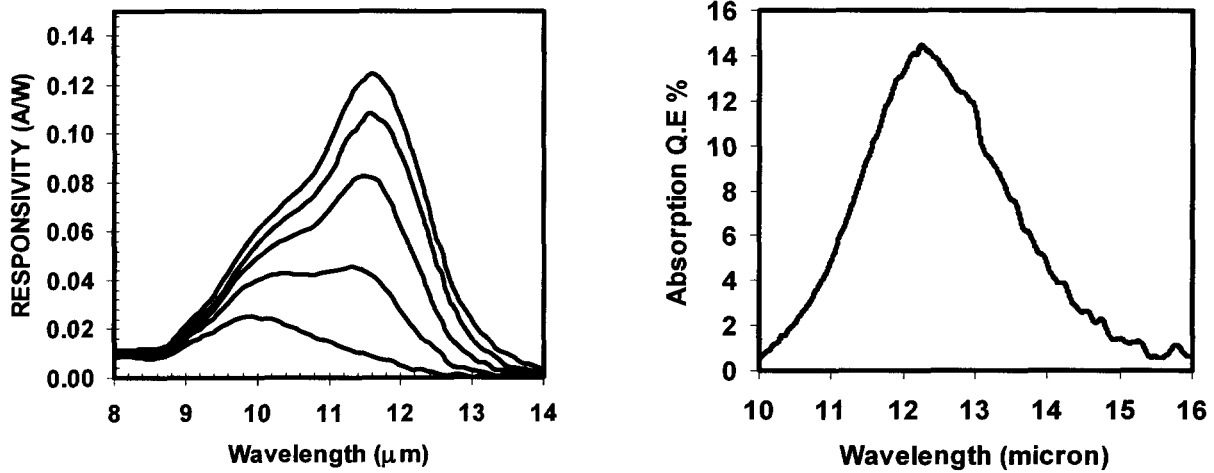


Fig. 10: Responsivity & absorption quantum efficiency spectra of the BID measured using a 45° wave guide geometry<sup>2</sup>. Shown responsivity curves are for different bias voltages from  $V_B = -0.5$  to 1.5 V with 0.25 V steps.

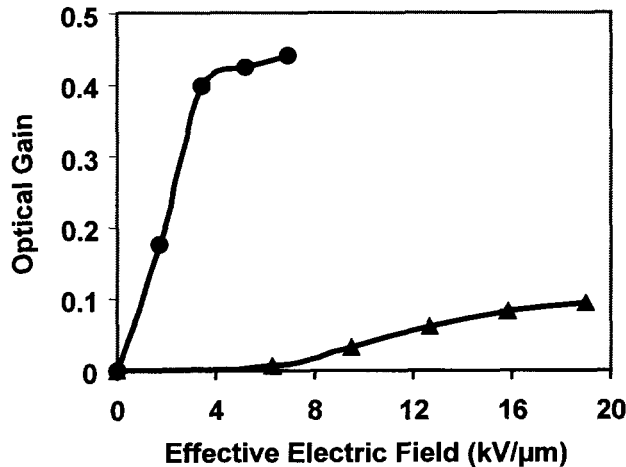


Fig. 11: Optical gain obtained for two different BID devices by measuring absorption quantum efficiency and responsivity. Improvement in optical gain is due to efficient carrier collection efficiency in the newest design.

blocked intersubband detector (BID) structure, with active superlattice and a thick blocking barrier, has been proposed to overcome this problem. Experimental measurements show similar absorption quantum efficiency, with a lower photoconductive gain. This can be attributed to a lower voltage drop across the active superlattice of the BID. The real advantage of the BID detector is that its infrared sensing photo emitter is a GaAs/AlGaAs based superlattice, thus, its cutoff wavelength can be easily tuned by band gap engineering (i.e, tailorable cutoff wavelengths). Therefore, if one seeks shorter wavelength operation such as 10 or 15 microns cutoff, the MQW based BID detectors will operate at much higher cryogenic temperatures such as 30 Kelvin which can be achieved passively at space low background conditions.

voltage drops across the blocking layer. Thus, the majority of the photoexcited electrons relax within the superlattice before reaching the blocking layer. In contrast, the typical QWIP has uniform resistivity along the active layer, which allows a substantial uniform electric field across the device. Figure 11 shows the comparison of optical gains for two different devices obtained by measuring absorption quantum efficiency and responsivity. Figure 12 shows dark currents measured at  $V = -1$  V bias voltage and at different operating temperatures. The estimated detectivity  $D^*$  at different operating temperatures, for a low background, with photon flux  $\phi = 4 \times 10^8$  photons/Sec/pixel is also illustrated in Fig. 12. This flux simulates 120 K space background with  $f/2$  -optics aperture.

## 6. CONCLUSION

We have demonstrated that QWIP is able to operate at low temperatures, with a higher sensitivity under high background irradiance levels. We also addressed the anomalous behavior of QWIP when operating under stringent low irradiance levels at low temperatures. A new

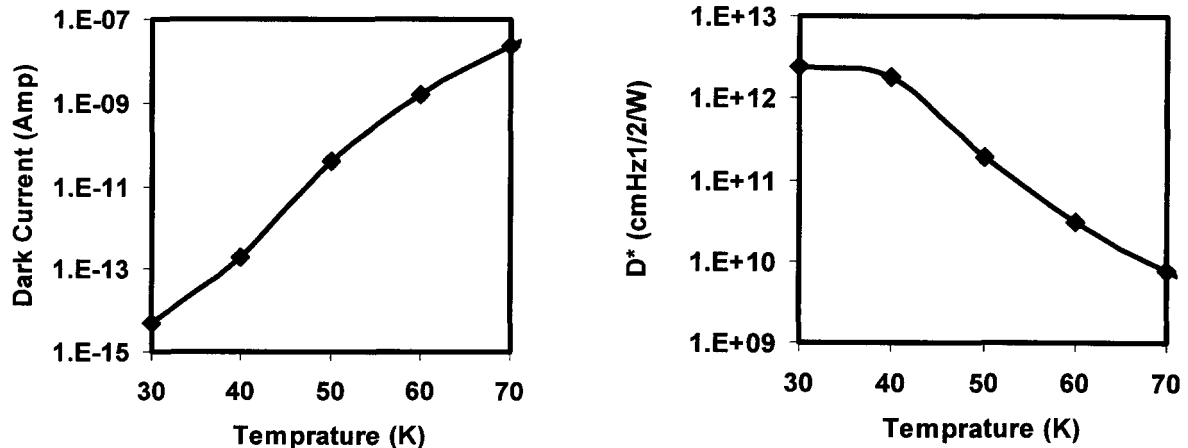


Fig. 12: BID dark current & Peak detectivity  $D^*$  vs operating temperature. The dark current was measured with 200  $\mu\text{m}$  diameter mesa & normalized to a  $30 \times 30 \mu\text{m}^2$  pixel.  $D^*$  is calculated based on responsivity & dark currents for a background with photon flux  $\phi = 4 \times 10^8$  photons/Sec/pixel which simulates 120 K space background and  $f/2$ -optics.

## 7. ACKNOWLEDGEMENT

The research described here was performed by the Center for Space Microelectronics Technology, Jet Propulsion Laboratory, California Institute of Technology, and was sponsored by the National Aeronautics and Space Administration, breakthrough sensor & instrument component technology thrust area of the cross enterprise technology development program.

## REFERENCES

1. S. D. Gunapala and S. V. Bandara, Physics of Thin Films, edited by M. H. Francombe, and J. L. Vossen, Vol. 21, pp. 113-237, Academic Press, NY, 1995.
2. B. F. Levine, J. Appl. Phys. **74**, R1 (1993).
3. S. D. Gunapala, S. V. Bandara, J. K. Liu, W. Hong, M. Sundaram, P. D. Maker, R. E. Muller, R. Carralejo, and C. A. Shott, IEEE Trans. Elec. Devices **45**, 1890 (1998).
4. S. D. Gunapala and S. V. Bandara, Quantum Well Infrared Photodetector (QWIP) Focal Plane Arrays, *Semiconductors and Semimetals*, 62, 197-282, Academic Press. 1999.
5. S. V. Bandara, et al. "10-16  $\mu\text{m}$  Broadband Quantum Well Infrared Photodetector", Appl. Phys. Lett., **72**, 2427 (1998).
6. S. Gunapala, S. Bandara, A. Singh, J. Liu, S. Rafol, E. Luong, J. Mumolo, N. Tran, J. Vincent, C. Shott, J. Long, and P. LeVan. 8-9 and 14-15  $\mu\text{m}$  Two-color 640x486 GaAs/AlGaAs Quantum Well Infrared Photodetector (QWIP) Focal Plane Array Camera, *SPIE* 3698, 687. 1999.
7. K. K. Choi, J. Appl. Phys. **80**, 1257 (1996).
8. H. C. Liu, Appl. Phys. Lett. **61**, 2703 (1992).
9. S. D. Gunapala, S. V. Bandara, A. Singh, J. K. Liu, E. M. Luong, J. M. Mumolo, M. J. McKelvey, Proc. SPIE, v.3379, 225 (1998).
10. M.W. Werner, et al. Paper 14.03 at San Diego AAS Meeting, 1998.
11. A. Singh and D. A. Cardimona, SPIE, Vol. **2999**, 46 (1997).
12. A. Singh and D. A. Cardimona, Opt. Eng. **38**, 1424 (1999).
13. D. C. Arrington, J. E. Hubbs, M. E. Gramer, Gary A. Dole, *SPIE* 4028, 288. 2000.
14. M. Ershov, S. Satou, and Y. Ikebe, J. Appl. Phys. **86**, 6442 (1999).
15. N. M. Haegel, C. R. Brennan, and A. M. White, J. Appl. Phys., **80**, 1510 (1996).